CHEMISTRY OF MATERIALS

pubs.acs.org/cm

Article

# Effect of Nonincorporative Cations on the Size and Shape of Indium Oxide Nanocrystals

Kihoon Kim, Lauren C. Reimnitz, Shin Hum Cho, Jungchul Noh, Ziyue Dong, Stephen L. Gibbs, Brian A. Korgel, and Delia J. Milliron*

Cite This: *Chem. Mater.* 2020, 32, 9347−9354

Read Online

ACCESS | Metrics & More | Article Recommendations | Supporting Information

**ABSTRACT:** A wide range of material properties can be accessed by tuning the size and shape of nanocrystals (NCs). Cations incorporated into the crystal lattice of indium oxide ($In_2O_3$) NCs as dopants have been shown to impact electronic, optical, and magnetic properties and also sometimes influence the NC shape, but the effects of nonincorporative cations have not been investigated. In this work, we found that nonincorporative alkali cations greatly affect the size and shape of $In_2O_3$ NCs. In particular, addition of sodium ions in the reactant mixture significantly increases the NC size and induces a rhombic dodecahedral (RDH) shape, which has not been observed in previous reports. By changing the volume of the precursor, we demonstrate size tunability from 17 to 45 nm, where shape is independently controlled by the sodium concentration. Finally, a progressive shape evolution from RDH to cubes is observed by incrementally replacing sodium in the precursor with potassium ions.

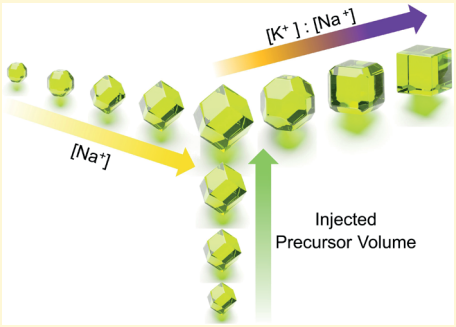




## 1. INTRODUCTION

The properties of colloidal inorganic nanocrystals (NCs), including optical, magnetic, electronic, and catalytic properties, are greatly influenced by their size and shape, suggesting opportunities for enabling applications not possible using poorly defined structures or bulk materials.[1−10] The shape- and size-dependent properties of many different metal oxide NC materials have been described and rationalized.[11−19] Indium oxide ($In_2O_3$) NCs offer a rich diversity of properties, including size- and shape-dependent photoluminescence, catalytic reactivity, and—with doped NCs such as tin-doped $In_2O_3$ ($Sn/In_2O_3$) and cerium-doped $In_2O_3$ ($Ce/In_2O_3$)—electronic conductivity and optical responses derived from localized surface plasmon resonance.[20−27] As a result of these past successes, there is now an abundance of information to achieve precise control over size and shape in many different material systems. Myriad shapes and sizes of various NCs have been synthesized and rationalized based on thermodynamic and kinetic principles.[24,27−33]

Still, independent control over a wide range of both size and shape is elusive with studies more typically demonstrating either size or shape control.[1,3−5,7,8,11−15,17−20] Inorganic NCs are commonly synthesized by heat-up or hot-injection methods in which all of the inorganic precursors are present from the outset of the reaction.[34] The reaction of the large amount of inorganic precursor can lead to a sudden increase of monomers to a high super saturation level. This super saturation results in nucleation and growth of NCs, where the size and shape of the NCs are determined by the kinetics of each reaction step.[28,34] Sometimes, facet-specific growth kinetics predicated that the relative surface energy of different crystal facets or chemistry between NCs and adsorptive molecules enables control of size and shape.[29−31] In this situation, it is difficult to separate the factors that control the size from those controlling shape, since their kinetics share many synthetic variables in common. Nonetheless, independent control over those two properties holds great promise not only for optimizing materials for particular applications but also for understanding the fundamental mechanisms underlying their synthesis.

As an alternative, synthetic strategies have been developed that take advantage of slow addition of inorganic precursors.[35−39] In a study of Ito et al., the synthesis of various metal oxides was demonstrated, including $In_2O_3$, iron (III) oxide, manganese (III) oxide, cobalt oxide, and zinc oxide by slowly injecting a metal carboxylate precursor into heated oleyl alcohol.[35] The size of the NCs was controlled by adjusting the injected volume of metal precursor solution with given concentration without changing experimental conditions that affect the reaction kinetics. This method enables precise control of NC size. However, since this method relies on

Received: August 11, 2020
Revised: August 19, 2020
Published: September 8, 2020





https://dx.doi.org/10.1021/acs.chemmater.0c03281
*Chem. Mater.* 2020, 32, 9347−9354

varying the quantity of the metal precursor, the size range that can be achieved is limited, for $In_2O_3$ to 16 nm, by the consumption of other reagents, especially oleyl alcohol.[35,38] The maximum size was extended by replenishing the oleyl alcohol and continuing the injection of $In^{3+}$ precursors, but the size was still limited to 22 nm.[38] Furthermore, since the concentration of metal precursors is low throughout the reaction, the shape of the metal oxide NCs tends to favor those that minimize surface energies, including icosahedra for iron oxide and rounded cubes for $In_2O_3$, usually without much shape control.[35] Because extending the available ranges of size and shape would offer more ways to optimize the properties of NCs, fundamental studies on the synthesis of metal oxide NCs with an eye toward increasing the NC diameter and producing varied shape are warranted. Such studies may also enable novel assembled structures, which will be useful to study interparticle interactions.[40−42]

In metal oxide NC synthesis, the introduction of dopants can affect the size and shape.[42−47,51,52] Most commonly, cations are incorporated into the host materials to change properties such as electronic conductivity, catalytic reactivity, and optical response.[25,26,48−51] Along with these changes, the introduction of dopants can alter the thermodynamics of nucleation and growth by modifying the facet-dependent surface energies, which is crucial in determining size and shape.[52] Jansons et al. found that cation dopant incorporation resulted in different sizes and shapes of doped $In_2O_3$ NCs because of changes in both surface energies of specific crystallographic facets and ligand−metal binding energy.[48] In the case of zinc oxide NCs, addition of magnesium was reported to change the crystal structure from wurtzite to zinc blende, which leads to different morphologies.[53]

While there are many studies on the influence of incorporative cations, few studies have explored the effect of nonincorporative cations on semiconductor NC synthesis. In the synthesis of magnetite ($Fe_3O_4$) NCs, substitution of sodium oleate (NaOL) or potassium oleate (KOL) for other oleate ligands has been found to change the shape from spheres to cubes.[8,13] This change was hypothesized to be caused by free oleate generated by the dissociation of the alkali metal oleate. Free oleate is known to bind preferentially to particular surfaces of the NCs in a way that depends strongly on the concentration of metal oleate in the reaction mixture. NaOL has also been shown to induce postsynthetic shape reconstruction of cadmium sulfide and cadmium selenide nanorods.[54]

Here, we systematically investigate the effect of non-incorporative cations on the synthesis of metal oxide NCs using a slow injection method. We focus on $In_2O_3$ NCs that have demonstrated plasmonic, catalytic, and electron conductive properties, all of which depend on size and shape.[25,27,55] The NC diameter increases monotonically with the increasing $Na^+$ concentration $[Na^+]$ for a given $In^{3+}$ precursor injection volume. The substitution of NaOL for oleic acid (OA) increases the diameter of the resulting NCs to more than twice that in a previous report[38] for the same amount of precursor. By increasing the volume of the precursor with a fixed $[Na^+]$, the largest NC diameter synthesized was 45 nm. Through analysis with high-resolution transmission electron microscope (HRTEM) and scanning electron microscope (SEM), we found that $Na^+$ induces rhombic dodecahedral (RDH) NCs, which have not been reported previously. Finally, by progressively changing the ratio of $Na^+$ to $K^+$, a corresponding progressive change in the NC shape was seen, from RDH to cubic, with well-defined transitional shapes like truncated RDH and truncated cube produced using intermediate mixtures of the alkali cations.

## 2. RESULTS AND DISCUSSION

To synthesize $In_2O_3$ NCs, first, the precursor solution was prepared by mixing indium acetate (InAc), OA, and 1-octadecene (ODE) in a three-neck flask at 160 °C. Based on prior reports, the molar ratio of $In^{3+}$ to organic ligands is expected to strongly impact the resulting NCs' size and shape.[56] Since the type of ligands affects the growth of NCs by changing surface energy and diffusivity of reagents,[28,57−59] we fixed the oleate concentration while introducing a variable amount of alkali cations. Specifically, OA was replaced by variable amounts of NaOL or KOL with the ratio between $In^{3+}$ and total oleate fixed at 1:6.33. Once this precursor solution was prepared, it was slowly injected into the reactor, which contained oleyl alcohol held at 290 °C. Previous studies suggest that the main reaction steps for $In_2O_3$ NC synthesis are (i) esterification between OA and oleyl alcohol, (ii) esterification between indium carboxylate and oleyl alcohol, and (iii) condensation of indium hydroxide, which is formed in reaction (ii) as shown in Supporting Information Figure S1.[35,38] Based on the stoichiometry in this model, the injected volume was fixed at 21 mL, since this amount was expected to consume all of the oleyl alcohol, and the corresponding $In^{3+}$ amount was 7 mmol.

First, we tested the effect of alkali cation concentration on the synthesis of $In_2O_3$ NCs. To preserve the ligand type as pure oleate, and because it has previously been shown to control the shape of $Fe_3O_4$ NCs, NaOL was used as the cation source.[8,13] The $[Na^+]$ was varied from 0 to 0.78 M, corresponding to substitution of OA by NaOL up to 37%. Concentrations of NaOL higher than this caused the solution to become supersaturated, resulting in the precipitation of reagents. The NC diameter was calculated using the area of projected images obtained by scanning transmission electron microscopy (STEM). For direct volume comparison, the shape of NCs was approximated as a sphere. In addition, at least 200 NCs were counted in each sample for statistical relevance. Increasing $[Na^+]$ from 0 to 0.78 M resulted in a linear increase in the NC diameter from 26 to 37 nm (Figure 1). Yield was measured by analyzing the $In^{3+}$ content in the NC products by digestion and analysis using inductively coupled plasma−atomic emission spectrometry (ICP-AES). The yield for each synthesis was almost identical, showing an average yield of 73 ± 3% (Supporting Information Figure S2). The projected shape of the NCs observed by STEM changes from pseudospherical to hexagonal, while the X-ray diffraction patterns exactly match the native $In_2O_3$ bixbyite crystal structure for all samples (Supporting Information Figure S3).

The reaction chemistry leading to the formation of $In_2O_3$ NCs was assessed using solution phase Fourier-transform infrared spectroscopy (FTIR) of aliquots collected through the entire synthetic process, from the preparation of precursor solutions to the injection of precursors into oleyl alcohol (Figure 2). To observe the role of $Na^+$, FTIR spectra for a reaction without $Na^+$ were compared to those for a reaction with $[Na^+]$ of 0.53 M. During preparation of precursor solution, the indium carboxylate peak is observed at 1570 $cm^{-1}$ (Figure 2a(i)). Unfortunately, this peak cannot be separated into $In^{3+}$ and $Na^+$ contributions, since the peaks due to the two


https://dx.doi.org/10.1021/acs.chemmater.0c03281
Chem. Mater. 2020, 32, 9347−9354

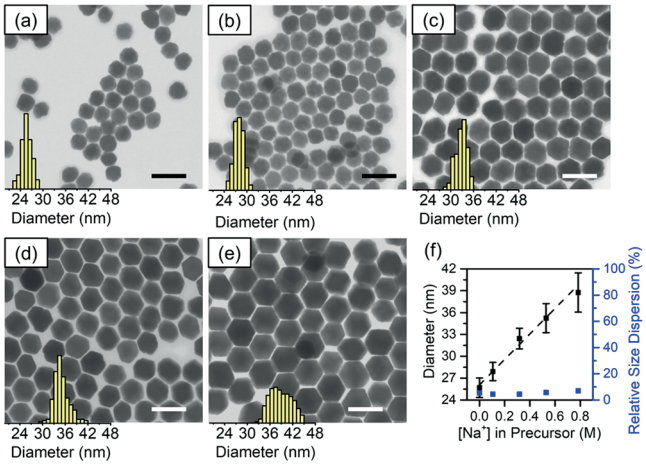


**Figure 1.** Size control of $In_2O_3$ NCs with varying $[Na^+]$. (panels a–e) STEM images of NCs synthesized using $[Na^+]$ of 0, 0.11, 0.32, 0.53, and 0.78 M in the precursor solutions, respectively. Inset histograms show the size distributions. Scale bars are 50 nm. (f) NC diameter and relative size dispersion dependence on $[Na^+]$ in precursor solution. Error bars indicate standard deviation based on image analysis. The dashed line represents fit.

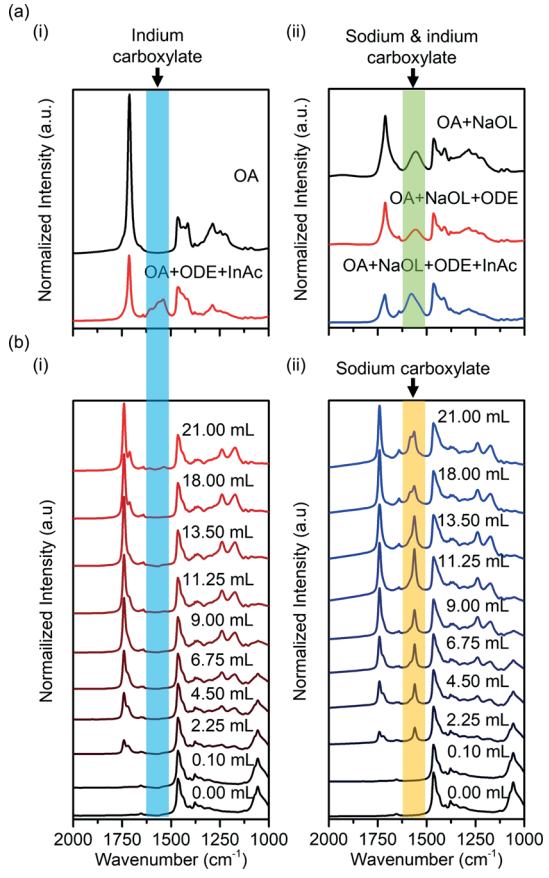


**Figure 2.** FTIR spectra of precursor solutions before injection and aliquots collected during injection of precursor solutions to oleyl alcohol. (a(i)) FTIR spectra during the preparation of precursor solution without $Na^+$ (a(ii)) and precursor solution with 0.53 M $Na^+$. (b(i)) After injection of the precursor without $Na^+$ (b(ii)) and precursor with $Na^+$. Labels indicate the volume of the precursor injected at the time of aliquot collection.

carboxylates overlap (Figure 2a(ii)). Then, FTIR spectra were collected during the NC synthesis by sampling aliquots after a known volume of precursor was injected (Figure 2b). All notable IR peaks are assigned in Table 1.

**Table 1. IR Peak Assignments**[56,60–62]

| wavenumber ($cm^{-1}$) | vibrational mode |
|---|---|
| 1064 | C–O stretch (alcohol) |
| 1175 | C–O stretch (ester) |
| 1241 | C–O stretch (ester) |
| 1462 | C–H bending |
| 1570 | asymmetric $COO^-$ stretch (metal carboxylate) |
| 1712 | C=O stretch (carboxylic acid) |
| 1741 | C=O stretch (ester) |

Regardless of the presence of $Na^+$, the injection of precursor solution caused the gradual disappearance of the alcohol O–H stretch at 3327 $cm^{-1}$, accompanied by the growth of the C=O stretch at 1741 $cm^{-1}$ (Figure 2 and Supporting Information Figure S4). These observations support the synthesis mechanism of $In_2O_3$ NCs based on esterification, as described in Supporting Information Figure S1. Notably, the signal at 1570 $cm^{-1}$ increased when NaOL was included in the precursor mixture, suggesting that either indium carboxylate or NaOL was accumulated in the reactor rather than being consumed in the production of metal oxide (Figure 2b(ii)). Because no accumulation of indium carboxylate was observed in the absence of NaOL (Figure 2b(i)) and $In^{3+}$ yields were identical regardless of $[Na^+]$, as shown in Supporting Information Figure S2, we conclude that this growth in signal is due to the accumulation of NaOL. Unlike the behavior of indium carboxylate, NaOL does not seem to consume oleyl alcohol to produce NaOH. Indeed, no hydroxyl species seem to accumulate, since FTIR shows only progressive disappearance of the O–H stretch intensity (Supporting Information Figure S4).[63] The finding that $Na^+$ is not incorporated into the NCs was further supported by the lack of Na signals in energy-dispersive X-ray spectroscopy (EDS) and X-ray photoelectron spectroscopy (XPS) analyses of the resulting NCs after purification (Supporting Information Figures S5 and S6). NaOL appears to be a spectator in the reaction mechanism.

Even though $Na^+$ appears not to directly participate in the reaction, the effect of $Na^+$ on NC size can be explained by the classical nucleation theory. The nucleation rate can be written in the form of an Arrhenius equation as follows:[29,34]

$$\frac{dN}{dt} = A\exp\left(\frac{-\Delta G_c}{k_b T}\right) \quad (1)$$

In this equation, $N$, $t$, $A$, $k_b$, and $T$ represent the number of nuclei, time, pre-exponential factor, Boltzmann's constant, and temperature, respectively. $\Delta G_c$ is the critical energy barrier for nucleation, and this can be further expressed as

$$\Delta G_c = \frac{16\pi\sigma^3\nu^2}{3k_b{}^2T^2(\ln S)^2} \quad (2)$$

Where, $\sigma$ and $\nu$ are defined as the surface energy of NCs and the molar volume of the monomer, and $S$ is supersaturation, which is defined as monomer concentration ($C$) divided by equilibrium monomer concentration ($C^*$).[29] According to eq 1, an increase in the surface energy will reduce the rate of nucleus formation. In a study of Agoston et al., the surface


https://dx.doi.org/10.1021/acs.chemmater.0c03281
Chem. Mater. 2020, 32, 9347–9354

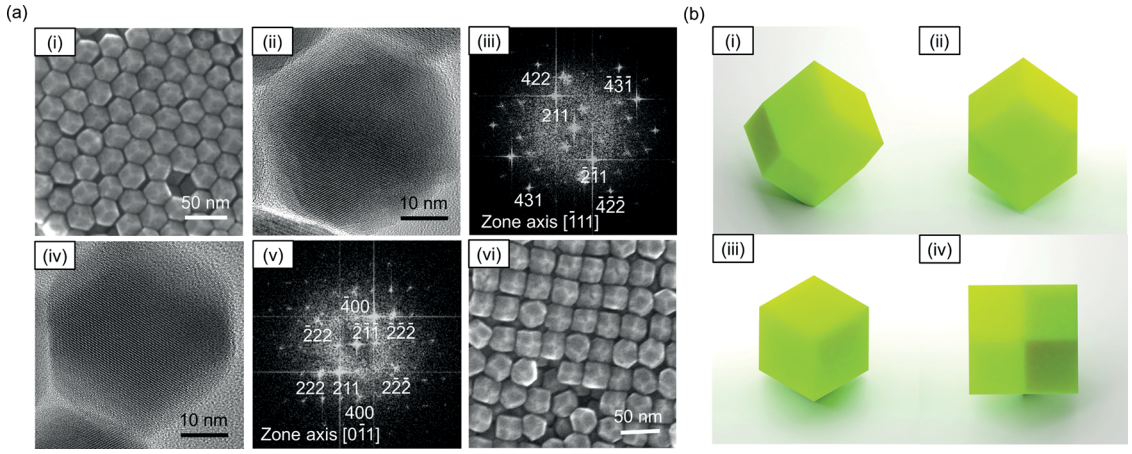


**Figure 3.** Shape analysis of $In_2O_3$ NCs synthesized with the precursor containing $Na^+$. (a(i)) SEM image of NCs with a regular hexagonal projection image, (a(ii)) HR-TEM image of regular hexagonal projection image, and (a(iii)) its FFT, which shows the [111] zone axis. (a(iv)) HR-TEM image and (a(v)) its FFT, which shows the [110] zone axis. All of the diffraction spots were indexed to the bixbyite crystal structure of $In_2O_3$. (a(vi)) SEM image of NCs aligned along the [100] direction. (b) Geometrical model of RDH in (i) a perspective view, (ii) [110] view, (iii) [111] view, and (iv) [100] view. $[Na^+]$ in precursor solution is 0.53 M.

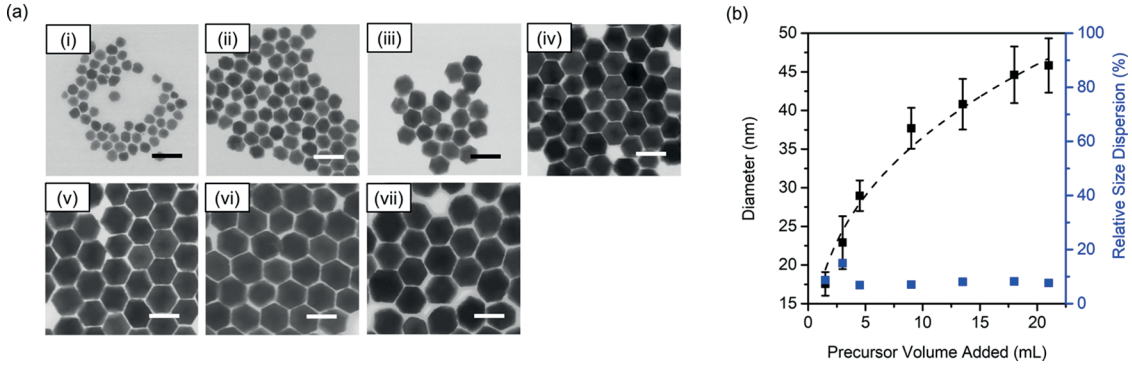


**Figure 4.** Size and shape investigation by changing the precursor amount and fixing the $[Na^+]$ in the precursor at 0.53 M. (a) SEM image of NCs synthesized with (i) 1.5, (ii) 3, (iii) 4.5, (iv) 9, (v) 13.5, (vi) 18, and (vii) 21 mL of precursor solution added. (b) NC diameter as a function of injected precursor volume. Scale bars are 50 nm. The dashed curve represents fit.

energy of $In_2O_3$ facets is reported to increase as $\sigma(111) < \sigma(110) < \sigma(100)$, but when the (100) facet is stabilized by water, it has a lower surface energy than (111).[64] Therefore, it can be deduced that a lower water concentration will decrease the number of nuclei by increasing the surface energy. Since water is mainly generated by the esterification reaction between free OA and oleyl alcohol, increasing the $[Na^+]$ by substituting OA for NaOL will reduce the water concentration in the reaction flask, causing an increase in NC size. Anecdotally, vigorous bumping occurs during this reaction, which can be ascribed to the boiling of water generated during NC synthesis. This bumping was seen to gradually decrease as $[Na^+]$ was increased. When NaOL was substituted with either sodium acetate (NaAc) or sodium octanoate (NaOc), for a given $[Na^+]$, the size of the resulting NCs is nearly identical (Supporting Information Figure S7). Moreover, the same size trend was observed using KOL instead of NaOL though KOL was seen to result in cubic NCs (Supporting Information Figure S8, further discussion below). Indeed, the alkali metal concentration in the precursor solution, which changes the amount of water produced in situ, is the main factor controlling the size of the NCs.

The shape of NCs was also seen to depend on the $[Na^+]$ in the precursor solution. While a pseudospherical shape formed without $Na^+$, a structure with sharp edges appearing hexagonal in projection resulted from a precursor solution containing 0.32 M or more $Na^+$ (Figure 1). The three-dimensional morphology of the NCs made with $[Na^+]$ of 0.53 M was analyzed by comparing SEM and HR-TEM images (Figure 3a). Depending on the orientation in a given region of the sample, the projected shapes observed are either regular hexagons with three edges on top, which intersect at 120° (Figure 3a(i)), or rectangular with four edges that cross perpendicularly (Figure 3a(vi)). Based on their HR-TEM images and fast Fourier transforms (FFT), the zone axis of the regular hexagonal projection is [111] (Figure 3a(ii) and (iii)). A NC of the same general hexagonal shape with a slightly different projection analyzed in this way indicated a zone axis of [110] (Figure 3(iv) and (v)). Comparison with the RDH shape model shown in Figure 3b reveals that the projection images of RDH from corresponding views match with the observations by electron microscopy exactly. Therefore, we conclude that the addition of $Na^+$ induces formation of RDH $In_2O_3$ NCs, passivated only by (110) facets. Various other nanomaterials, including gold, palladium, copper oxide, and $Fe_3O_4$, have been observed with RDH shape but not $In_2O_3$.[11,65−67]


https://dx.doi.org/10.1021/acs.chemmater.0c03281
Chem. Mater. 2020, 32, 9347−9354

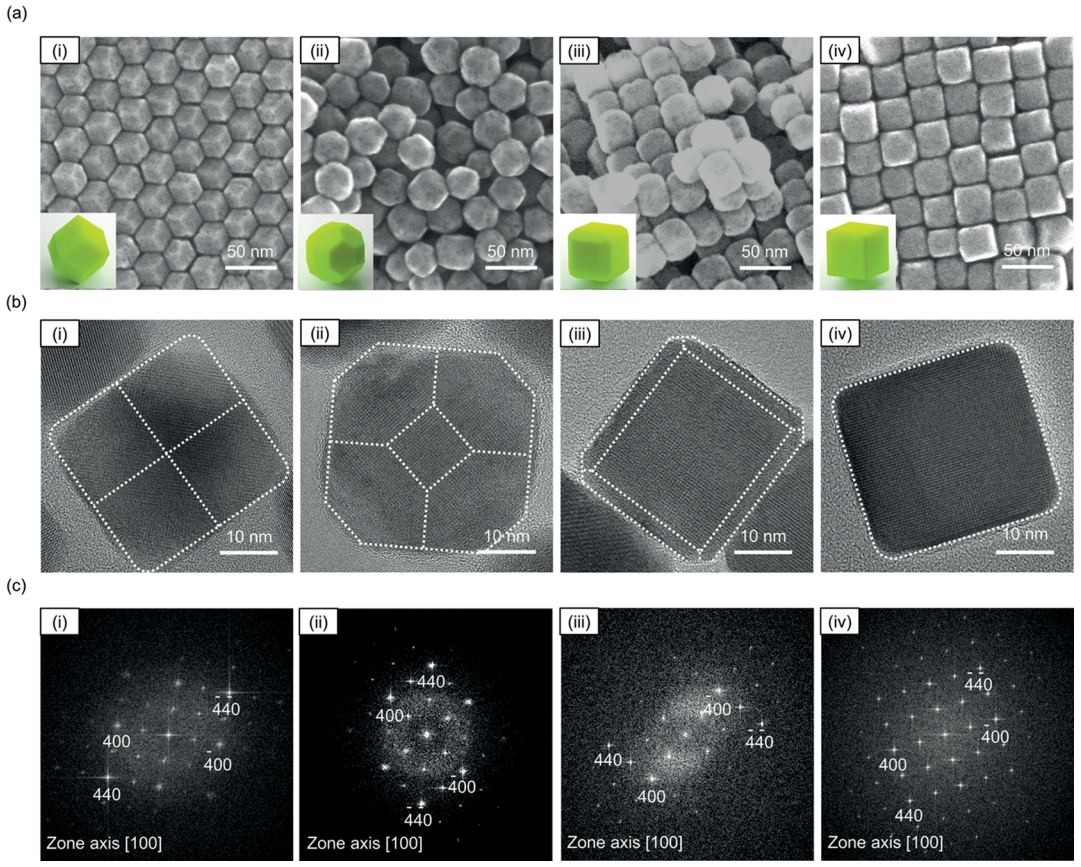


**Figure 5.** Shape evolution when substituting cations from $Na^+$ to $K^+$. (a) SEM images of NCs made with precursors containing (i) [$Na^+$] 0.53 M, (ii) [$Na^+$] 0.27 M and [$K^+$] 0.27 M, (iii) [$Na^+$] 0.11 M and [$K^+$] 0.42 M, and (iv) [$K^+$] 0.53 M. (b) HR-TEM images of NCs synthesized with precursors containing (i) [$Na^+$] 0.53 M, (ii) [$Na^+$] 0.27 M and [$K^+$] 0.27 M, (iii) [$Na^+$] 0.11 M and [$K^+$] 0.42 M, and (iv) [$K^+$] 0.53 M. (c) FFT of respective HR-TEM shown in (b). The diffraction spots were indexed to the bixbyite crystal structure of $In_2O_3$.

Although the inclusion of NaOL increases the accessible size range for $In_2O_3$ NCs, we sought to extend this even further by varying the injected volume of precursor solution with [$Na^+$] fixed at 0.53 M (Figure 4). Aliquots were taken to analyze the NC size and shape. The size of the NCs gradually increased, maintaining the RDH shape (Figure 4a), suggesting that shape is determined by the ratio of OA and NaOL in the precursor, rather than the total NaOL amount. The diameter of the NCs increased from 17 to 45 nm, varying as the cube root of the injected volume, while maintaining only 10% relative size dispersion (Figure 4b). In other words, the volume of each NC varies linearly with the quantity of the precursor injected. This scaling—along with the narrow size distribution—supports the conclusions of a previous report that the continuous injection method promotes the formation of seed particles near the beginning of the precursor injection while suppressing secondary homogeneous nucleation.[38] For 7 mmol of $In^{3+}$ added, the $In_2O_3$ NC diameter was increased by approximately 3 times (almost 10 times in volume) by our protocol including $Na^+$ in the precursor solution compared to previous reports using slow injection. Our use of ODE to reduce the viscosity also increases the size of NCs compared to that previously reported.[38] This can be attributed to the increase of critical energy for nucleation because addition of ODE will decrease the supersaturation as described in eq 2. Since it has been shown that NCs can be grown even larger by replenishing oleyl alcohol, we can expect that the maximum size achievable by combining these strategies may be substantially larger than this.[38]

The role of the spectator cation in determining the particle shape was studied by substituting $Na^+$ with $K^+$ (Figure 5). Reactions were performed by fixing the concentration of total nonincorporative cations in the precursor at 0.53 M while changing the ratio of $Na^+$ to $K^+$. Hence, the [$Na^+$] decreased as 0.53, 0.27, 0.11, to 0 M, compensated by increasing [$K^+$] of 0, 0.27, 0.42, and 0.53 M, respectively. As discussed previously, RDH $In_2O_3$ NCs were produced with precursors including $Na^+$ (Figure 5a(i)). Incrementally substituting [$K^+$] induces a change in the NC morphology (Figure 5a(ii,iii)), and fully substituting with $K^+$ resulted in cubic NCs (Figure 5a(iv)). The NC shape was determined by HR-TEM (Figure 5b). HR-TEM images with the zone axis [100] were selected to compare morphological evolution according to the cation composition. While $Na^+$ in the precursor solution caused the preferential expression of (110) faces on the resulting NCs, $K^+$ promotes the expression of (100) facets. For this reason, NCs are shown to gradually change shape from pure RDH to (100)-truncated RDH to (110)-truncated cubes, and ultimately, to pure cubes with (100)-terminated faces. This shape evolution is not explainable by the same shape control mechanism suggested by previous work on $Fe_3O_4$ NCs, since the shape evolution seen here was only dependent on the sort of cation and not concentration (Figure 2 and Supporting Information Figure S8).[13]


https://dx.doi.org/10.1021/acs.chemmater.0c03281
Chem. Mater. 2020, 32, 9347−9354

Highly faceted particles have been grown by selective adsorption of molecules onto specific crystal facets.[24,28,29] In our case, $Na^+$ and $K^+$ are not detected by EDS or XPS for any of the conditions used in this work, even though the concentration of nonincorporative cations is 1.6 times higher than that of $In^{3+}$ (Supporting Information Figure S5). This indicates that $Na^+$ and $K^+$ are not incorporated in the $In_2O_3$ NCs or bound to the surface (Supporting Information Figure S6). Since the facets are not caused by selective adsorption of our alkali metal ions and considering the previous report that metal oleate promotes the reconstruction of NC surfaces, we hypothesize that these spectators instead change surface thermodynamics in another way to induce stabilization of different crystal facets.[27,54]

Metal oleates are amphiphilic ion pairs that dissociate when heated to generate a cation and a free oleate, as shown by conductivity measurements in previous reports.[13,68,69] According to these studies, the extent of dissociation is much greater for KOL than for NaOL, driven mainly by the ionic radius of each cation that makes the $K^+$−oleate interaction substantially weaker than that between $Na^+$ and oleate.[69] The extent of dissociation determines the concentration of charged free oleate, which affects the polarity of the synthesis environment and, in turn, the relative surface energies of different crystal facets. Since $K^+$ is expected to dissociate from oleate to a greater extent, precursor solutions made with KOL would be more polar than those made with NaOL, promoting the presence of the more polar (100) facets. The series of transitional shapes obtained by mixing NaOL and KOL can be explained based on a continuous variation in solution polarity, since the average surface polarity of each shape is between that of pure RDH and pure cube following the Wulff construction rule.[28,70,71]

## 3. CONCLUSIONS

In conclusion, we systemically studied the effect of non-incorporative cations on the shape and size of $In_2O_3$ NCs. The concentration of alkali metal cations affects the NC size by reducing the amount of water generated during synthesis, which can stabilize the surface of metal oxide NCs. The shape of the NCs was shown to change gradually from the pseudosphere to RDH, as $[Na^+]$ was increased. The faceted shape could be tuned from RDH to cubes by changing the ratio of $K^+$ to $Na^+$, which very precisely controls the relative expression of the (110) and (100) facets. Continuous size control was also possible by adjusting the volume of precursor solution injected during synthesis. This synthesis innovation offers improved control over NC size and shape compared to previous methods. In accordance with the features of injection syntheses demonstrated in previous reports, we expect that this method can be adapted to the synthesis of other metal oxide NCs and heterostructures to result in a vast array of sizes, shapes, and compositions. We hope that the insights we gain here provide tools for optimizing both the useful properties of discrete NCs and the collective properties that stem from various shape- and size-dependent assemblies.

## ■ ASSOCIATED CONTENT

### Supporting Information

The Supporting Information is available free of charge at https://pubs.acs.org/doi/10.1021/acs.chemmater.0c03281.

Experimental procedure, spectral data, composition analysis data, and STEM/SEM data (PDF)

## ■ AUTHOR INFORMATION


### Corresponding Author

**Delia J. Milliron** − *McKetta Department of Chemical Engineering, The University of Texas at Austin, Austin, Texas 78712, United States;* orcid.org/0000-0002-8737-451X; Email: milliron@che.utexas.edu

### Authors

**Kihoon Kim** − *McKetta Department of Chemical Engineering, The University of Texas at Austin, Austin, Texas 78712, United States;* orcid.org/0000-0003-1034-9233

**Lauren C. Reimnitz** − *McKetta Department of Chemical Engineering, The University of Texas at Austin, Austin, Texas 78712, United States*

**Shin Hum Cho** − *McKetta Department of Chemical Engineering, The University of Texas at Austin, Austin, Texas 78712, United States; Samsung Electronics, Samsung Semiconductor R&D, Hwaseong, Gyeonggi-do 18448, Republic of Korea;* orcid.org/0000-0002-0271-116X

**Jungchul Noh** − *McKetta Department of Chemical Engineering and Texas Materials Institute, The University of Texas at Austin, Austin, Texas 78712, United States*

**Ziyue Dong** − *McKetta Department of Chemical Engineering, The University of Texas at Austin, Austin, Texas 78712, United States*

**Stephen L. Gibbs** − *McKetta Department of Chemical Engineering, The University of Texas at Austin, Austin, Texas 78712, United States;* orcid.org/0000-0003-2533-0957

**Brian A. Korgel** − *McKetta Department of Chemical Engineering and Texas Materials Institute, The University of Texas at Austin, Austin, Texas 78712, United States;* orcid.org/0000-0001-6242-7526

Complete contact information is available at: https://pubs.acs.org/10.1021/acs.chemmater.0c03281


### Author Contributions

All authors have given approval to the final version of the manuscript.

### Notes

The authors declare no competing financial interest.

## ■ ACKNOWLEDGMENTS

This research was primarily supported by the Center for Dynamics and Control of Materials, a National Science Foundation Materials Research Science and Engineering Center (NSF MRSEC DMR-1720595). Additional support was provided by NSF (CHE-1905263), the Robert A. Welch Foundation (F-1848 & F-1464), Lockheed Martin (UTA 19-000624), the Fulbright Program (IIE-15151071 to S.H.C.), and an NSF Graduate Research Fellowship (DGE-1610403 to S.L.G).

## ■ REFERENCES

(1) Sun, S.; Murray, C. B.; Weller, D.; Folks, L.; Moser, A. Monodisperse FePt Nanoparticles and Ferromagnetic FePt Nanocrystal Superlattices. *Science* **2000**, *287*, 1989−1992.

(2) Colvin, V. L.; Schlamp, M. C.; Alivisatos, A. P. Light-Emitting Diodes Made from Cadmium Selenide Nanocrystals and a Semiconducting Polymer. *Nature* **1994**, *370*, 354−357.

(3) Puntes, V. F.; Zanchet, D.; Erdonmez, C. K.; Alivisatos, A. P. Synthesis of Hcp-Co Nanodisks. *J. Am. Chem. Soc.* **2002**, *124*, 12874−12880.
(4) An, K.; Somorjai, G. A. Size and Shape Control of Metal Nanoparticles for Reaction Selectivity in Catalysis. *ChemCatChem* **2012**, *4*, 1512−1524.
(5) Somorjai, G. A. Modern Surface Science and Surface Technologies: An Introduction. *Chem. Rev.* **1996**, *96*, 1223−1236.
(6) Jeong, S.; Woo, K.; Kim, D.; Lim, S.; Kim, J. S.; Shin, H.; Xia, Y.; Moon, J. Controlling the Thickness of the Surface Oxide Layer on Cu Nanoparticles for the Fabrication of Conductive Structures by Ink-Jet Printing. *Adv. Funct. Mater.* **2008**, *18*, 679−686.
(7) Li, W.; Zamani, R.; Rivera Gil, P.; Pelaz, B.; Ibáñez, M.; Cadavid, D.; Shavel, A.; Alvarez-Puebla, R. A.; Parak, W. J.; Arbiol, J.; Cabot, A. CuTe Nanocrystals: Shape and Size Control, Plasmonic Properties, and Use as SERS Probes and Photothermal Agents. *J. Am. Chem. Soc.* **2013**, *135*, 7098−7101.
(8) Roca, A. G.; Gutiérrez, L.; Gavilán, H.; Fortes Brollo, M. E.; Veintemillas-Verdaguer, S.; Morales, M. D. P. Design Strategies for Shape-Controlled Magnetic Iron Oxide Nanoparticles. *Adv. Drug Delivery Rev.* **2019**, *138*, 68−104.
(9) Kim, K.; Han, H. S.; Choi, I.; Lee, C.; Hong, S.; Suh, S.-H.; Lee, L. P.; Kang, T. Interfacial Liquid-State Surface-Enhanced Raman Spectroscopy. *Nat. Commun.* **2013**, *4*, 2182.
(10) Jeong, E.; Kim, K.; Choi, I.; Jeong, S.; Park, Y.; Lee, H.; Kim, S. H.; Lee, L. P.; Choi, Y.; Kang, T. Three-Dimensional Reduced-Symmetry of Colloidal Plasmonic Nanoparticles. *Nano Lett.* **2012**, *12*, 2436−2440.
(11) Huang, W.-C.; Lyu, L.-M.; Yang, Y.-C.; Huang, M. H. Synthesis of $Cu_2O$ Nanocrystals from Cubic to Rhombic Dodecahedral Structures and Their Comparative Photocatalytic Activity. *J. Am. Chem. Soc.* **2012**, *134*, 1261−1267.
(12) Grassian, V. H. When Size Really Matters: Size-Dependent Properties and Surface Chemistry of Metal and Metal Oxide Nanoparticles in Gas and Liquid Phase Environments. *J. Phys. Chem. C* **2008**, *112*, 18303−18313.
(13) Kovalenko, M. V.; Bodnarchuk, M. I.; Lechner, R. T.; Hesser, G.; Schäffler, F.; Heiss, W. Fatty Acid Salts as Stabilizers in Size- and Shape-Controlled Nanocrystal Synthesis: The Case of Inverse Spinel Iron Oxide. *J. Am. Chem. Soc.* **2007**, *129*, 6352−6353.
(14) Sadasivan, S.; Bellabarba, R. M.; Tooze, R. P. Size Dependent Reduction−Oxidation−Reduction Behaviour of Cobalt Oxide Nanocrystals. *Nanoscale* **2013**, *5*, 11139−11146.
(15) Pu, Y.-J.; Morishita, N.; Chiba, T.; Ohisa, S.; Igarashi, M.; Masuhara, A.; Kido, J. Efficient Electron Injection by Size- and Shape-Controlled Zinc Oxide Nanoparticles in Organic Light-Emitting Devices. *ACS Appl. Mater. Interfaces* **2015**, *7*, 25373−25377.
(16) Roy, N.; Sohn, Y.; Pradhan, D. Synergy of Low-Energy {101} and High-Energy {001} $TiO_2$ Crystal Facets for Enhanced Photocatalysis. *ACS Nano* **2013**, *7*, 2532−2540.
(17) Kwak, J. H.; Tonkyn, R.; Tran, D.; Mei, D.; Cho, S. J.; Kovarik, L.; Lee, J. H.; Peden, C. H. F.; Szanyi, J. Size-Dependent Catalytic Performance of CuO on $\gamma$-$Al_2O_3$: NO Reduction versus $NH_3$ Oxidation. *ACS Catal.* **2012**, *2*, 1432−1440.
(18) Seo, W. S.; Jo, H. H.; Lee, K.; Kim, B.; Oh, S. J.; Park, J. T. Size-Dependent Magnetic Properties of Colloidal $Mn_3O_4$ and MnO Nanoparticles. *Angew. Chem., Int. Ed.* **2004**, *43*, 1115−1117.
(19) Gordon, T. R.; Paik, T.; Klein, D. R.; Naik, G. V.; Caglayan, H.; Boltasseva, A.; Murray, C. B. Shape-Dependent Plasmonic Response and Directed Self-Assembly in a New Semiconductor Building Block, Indium-Doped Cadmium Oxide (ICO). *Nano Lett.* **2013**, *13*, 2857−2863.
(20) Crockett, B. M.; Jansons, A. W.; Koskela, K. M.; Sharps, M. C.; Johnson, D. W.; Hutchison, J. E. Influence of Nanocrystal Size on the Optoelectronic Properties of Thin, Solution-Cast Sn-Doped $In_2O_3$ Films. *Chem. Mater.* **2019**, *31*, 3370−3380.
(21) Murali, A.; Barve, A.; Leppert, V. J.; Risbud, S. H.; Kennedy, I. M.; Lee, H. W. H. Synthesis and Characterization of Indium Oxide Nanoparticles. *Nano Lett.* **2001**, *1*, 287−289.
(22) Han, X.; Han, X.; Sun, L.; Gao, S.; Li, L.; Kuang, Q.; Xie, Z.; Wang, C. Synthesis of Trapezohedral Indium Oxide Nanoparticles with High-Index {211} Facets and High Gas Sensing Activity. *Chem. Commun.* **2015**, *51*, 9612−9615.
(23) Zandi, O.; Agrawal, A.; Shearer, A. B.; Reimnitz, L. C.; Dahlman, C. J.; Staller, C. M.; Milliron, D. J. Impacts of Surface Depletion on the Plasmonic Properties of Doped Semiconductor Nanocrystals. *Nat. Mater.* **2018**, *17*, 710−717.
(24) Cho, S. H.; Ghosh, S.; Berkson, Z. J.; Hachtel, J. A.; Shi, J.; Zhao, X.; Reimnitz, L. C.; Dahlman, C. J.; Ho, Y.; Yang, A.; Liu, Y.; Idrobo, J.-C.; Chmelka, B. F.; Milliron, D. J. Syntheses of Colloidal F:$In_2O_3$ Cubes: Fluorine-Induced Faceting and Infrared Plasmonic Response. *Chem. Mater.* **2019**, *31*, 2661−2676.
(25) Kim, B. H.; Staller, C. M.; Cho, S. H.; Heo, S.; Garrison, C. E.; Kim, J.; Milliron, D. J. High Mobility in Nanocrystal-Based Transparent Conducting Oxide Thin Films. *ACS Nano* **2018**, *12*, 3200−3208.
(26) Staller, C. M.; Gibbs, S. L.; Saez Cabezas, C. A.; Milliron, D. J. Quantitative Analysis of Extinction Coefficients of Tin-Doped Indium Oxide Nanocrystal Ensembles. *Nano Lett.* **2019**, *19*, 8149−8154.
(27) Agrawal, A.; Cho, S. H.; Zandi, O.; Ghosh, S.; Johns, R. W.; Milliron, D. J. Localized Surface Plasmon Resonance in Semiconductor Nanocrystals. *Chem. Rev.* **2018**, *118*, 3121−3207.
(28) Xia, Y.; Xiong, Y.; Lim, B.; Skrabalak, S. E. Shape-Controlled Synthesis of Metal Nanocrystals: Simple Chemistry Meets Complex Physics? *Angew. Chem., Int. Ed.* **2009**, *48*, 60−103.
(29) Wu, Z.; Yang, S.; Wu, W. Shape Control of Inorganic Nanoparticles from Solution. *Nanoscale* **2016**, *8*, 1237−1259.
(30) Lin, H.; Lei, Z.; Jiang, Z.; Hou, C.; Liu, D.; Xu, M.; Tian, Z.; Xie, Z. Supersaturation-Dependent Surface Structure Evolution: From Ionic, Molecular to Metallic Micro/Nanocrystals. *J. Am. Chem. Soc.* **2013**, *135*, 9311−9314.
(31) Lai, W.-H.; Wang, Y.-X.; Wang, Y.; Wu, M.; Wang, J.-Z.; Liu, H.-K.; Chou, S.-L.; Chen, J.; Dou, S.-X. Morphology Tuning of Inorganic Nanomaterials Grown by Precipitation through Control of Electrolytic Dissociation and Supersaturation. *Nat. Chem.* **2019**, *11*, 695−701.
(32) Ghosh, S.; Manna, L. The Many "Facets" of Halide Ions in the Chemistry of Colloidal Inorganic Nanocrystals. *Chem. Rev.* **2018**, *118*, 7804−7864.
(33) Figueroa-Cosme, L.; Park, J.; Bao, S.; Xia, Y. Seed-Mediated Growth of Colloidal Metal Nanocrystals: Scaling up the Production through Geometric and Stoichiometric Analyses. *ChemNanoMat* **2016**, *2*, 1033−1039.
(34) Kwon, S. G.; Hyeon, T. Formation Mechanisms of Uniform Nanocrystals via Hot-Injection and Heat-Up Methods. *Small* **2011**, *7*, 2685−2702.
(35) Ito, D.; Yokoyama, S.; Zaikova, T.; Masuko, K.; Hutchison, J. E. Synthesis of Ligand-Stabilized Metal Oxide Nanocrystals and Epitaxial Core/Shell Nanocrystals via a Lower-Temperature Esterification Process. *ACS Nano* **2014**, *8*, 64−75.
(36) Franke, D.; Harris, D. K.; Chen, O.; Bruns, O. T.; Carr, J. A.; Wilson, M. W. B.; Bawendi, M. G. Continuous Injection Synthesis of Indium Arsenide Quantum Dots Emissive in the Short-Wavelength Infrared. *Nat. Commun.* **2016**, *7*, 1−9.
(37) Wainer, P.; Kendall, O.; Lamb, A.; Barrow, S. J.; Tricoli, A.; Gómez, D. E.; van Embden, J.; Della Gaspera, E. Continuous Growth Synthesis of Zinc Oxide Nanocrystals with Tunable Size and Doping. *Chem. Mater.* **2019**, *31*, 9604−9613.
(38) Jansons, A. W.; Hutchison, J. E. Continuous Growth of Metal Oxide Nanocrystals: Enhanced Control of Nanocrystal Size and Radial Dopant Distribution. *ACS Nano* **2016**, *10*, 6942−6951.
(39) Shieh, F.; Saunders, A. E.; Korgel, B. A. General Shape Control of Colloidal CdS, CdSe, CdTe Quantum Rods and Quantum Rod Heterostructures. *J. Phys. Chem. B* **2005**, *109*, 8538−8542.
(40) Wang, T.; Zhuang, J.; Lynch, J.; Chen, O.; Wang, Z.; Wang, X.; LaMontagne, D.; Wu, H.; Wang, Z.; Cao, Y. C. Self-Assembled Colloidal Superparticles from Nanorods. *Science* **2012**, *338*, 358−363.


https://dx.doi.org/10.1021/acs.chemmater.0c03281
*Chem. Mater.* 2020, 32, 9347−9354

(41) Ye, X.; Chen, J.; Engel, M.; Millan, J. A.; Li, W.; Qi, L.; Xing, G.; Collins, J. E.; Kagan, C. R.; Li, J.; Glotzer, S. C.; Murray, C. B. Competition of Shape and Interaction Patchiness for Self-Assembling Nanoplates. *Nat. Chem.* **2013**, *5*, 466−473.
(42) Henzie, J.; Grünwald, M.; Widmer-Cooper, A.; Geissler, P. L.; Yang, P. Self-Assembly of Uniform Polyhedral Silver Nanocrystals into Densest Packings and Exotic Superlattices. *Nat. Mater.* **2012**, *11*, 131−137.
(43) Della Gaspera, E.; Chesman, A. S. R.; van Embden, J.; Jasieniak, J. J. Non-Injection Synthesis of Doped Zinc Oxide Plasmonic Nanocrystals. *ACS Nano* **2014**, *8*, 9154−9163.
(44) Schwartz, D. A.; Norberg, N. S.; Nguyen, Q. P.; Parker, J. M.; Gamelin, D. R. Magnetic Quantum Dots: Synthesis, Spectroscopy, and Magnetism of $Co^{2+}$- and $Ni^{2+}$-Doped ZnO Nanocrystals. *J. Am. Chem. Soc.* **2003**, *125*, 13205−13218.
(45) van Enckevort, W. J. P.; van der Berg, A. C. J. F.; Kreuwel, K. B. G.; Derksen, A. J.; Couto, M. S. Impurity Blocking of Growth Steps: Experiments and Theory. *J. Cryst. Growth* **1996**, *166*, 156−161.
(46) Buonsanti, R.; Milliron, D. J. Chemistry of Doped Colloidal Nanocrystals. *Chem. Mater.* **2013**, *25*, 1305−1317.
(47) Mehra, S.; Bergerud, A.; Milliron, D. J.; Chan, E. M.; Salleo, A. Core/Shell Approach to Dopant Incorporation and Shape Control in Colloidal Zinc Oxide Nanorods. *Chem. Mater.* **2016**, *28*, 3454−3461.
(48) Jansons, A. W.; Koskela, K. M.; Crockett, B. M.; Hutchison, J. E. Transition Metal-Doped Metal Oxide Nanocrystals: Efficient Substitutional Doping through a Continuous Growth Process. *Chem. Mater.* **2017**, *29*, 8167−8176.
(49) Staller, C. M.; Robinson, Z. L.; Agrawal, A.; Gibbs, S. L.; Greenberg, B. L.; Lounis, S. D.; Kortshagen, U. R.; Milliron, D. J. Tuning Nanocrystal Surface Depletion by Controlling Dopant Distribution as a Route Toward Enhanced Film Conductivity. *Nano Lett.* **2018**, *18*, 2870−2878.
(50) Song, H.; Hong, J. A.; Lee, H.; Lim, K. Comparative Study on the Catalytic Activity of Fe-Doped $ZrO_2$ Nanoparticles without Significant Toxicity through Chemical Treatment under Various PH Conditions. *Sci. Rep.* **2019**, *9*, 1−13.
(51) Tandon, B.; Ghosh, S.; Milliron, D. J. Dopant Selection Strategy for High-Quality Factor Localized Surface Plasmon Resonance from Doped Metal Oxide Nanocrystals. *Chem. Mater.* **2019**, *31*, 7752−7760.
(52) Bryan, J. D.; Gamelin, D. R. Doped Semiconductor Nanocrystals: Synthesis, Characterization, Physical Properties, and Applications. *In Progress in Inorganic Chemistry*; John Wiley & Sons, Ltd, 2005; 47−126.
(53) Yang, Y.; Jin, Y.; He, H.; Wang, Q.; Tu, Y.; Lu, H.; Ye, Z. Dopant-Induced Shape Evolution of Colloidal Nanocrystals: The Case of Zinc Oxide. *J. Am. Chem. Soc.* **2010**, *132*, 13381−13394.
(54) Oh, N.; Shim, M. Metal Oleate Induced Etching and Growth of Semiconductor Nanocrystals, Nanorods, and Their Heterostructures. *J. Am. Chem. Soc.* **2016**, *138*, 10444−10451.
(55) Martin, O.; Martín, A. J.; Mondelli, C.; Mitchell, S.; Segawa, T. F.; Hauert, R.; Drouilly, C.; Curulla-Ferré, D.; Pérez-Ramírez, J. Indium Oxide as a Superior Catalyst for Methanol Synthesis by $CO_2$ Hydrogenation. *Angew. Chem., Int. Ed.* **2016**, *55*, 6261−6265.
(56) Narayanaswamy, A.; Xu, H.; Pradhan, N.; Kim, M.; Peng, X. Formation of Nearly Monodisperse $In_2O_3$ Nanodots and Oriented-Attached Nanoflowers: Hydrolysis and Alcoholysis vs Pyrolysis. *J. Am. Chem. Soc.* **2006**, *128*, 10310−10319.
(57) Yu, W. W.; Wang, Y. A.; Peng, X. Formation and Stability of Size-, Shape-, and Structure-Controlled CdTe Nanocrystals: Ligand Effects on Monomers and Nanocrystals. *Chem. Mater.* **2003**, *15*, 4300−4308.
(58) Bealing, C. R.; Baumgardner, W. J.; Choi, J. J.; Hanrath, T.; Hennig, R. G. Predicting Nanocrystal Shape through Consideration of Surface-Ligand Interactions. *ACS Nano* **2012**, *6*, 2118−2127.
(59) Mokari, T.; Zhang, M.; Yang, P. Shape, Size, and Assembly Control of PbTe Nanocrystals. *J. Am. Chem. Soc.* **2007**, *129*, 9864−9865.
(60) Chang, H.; Kim, B. H.; Jeong, H. Y.; Moon, J. H.; Park, M.; Shin, K.; Chae, S. I.; Lee, J.; Kang, T.; Choi, B. K.; Yang, J.; Bootharaju, M. S.; Song, H.; An, S. H.; Park, K. M.; Oh, J. Y.; Lee, H.; Kim, M. S.; Park, J.; Hyeon, T. Molecular-Level Understanding of Continuous Growth from Iron-Oxo Clusters to Iron Oxide Nanoparticles. *J. Am. Chem. Soc.* **2019**, *141*, 7037−7045.
(61) Singhal, A.; Pai, M. R.; Rao, R.; Pillai, K. T.; Lieberwirth, I.; Tyagi, A. K. Copper(I) Oxide Nanocrystals − One Step Synthesis, Characterization, Formation Mechanism, and Photocatalytic Properties. *Eur. J. Inorg. Chem.* **2013**, *2013*, 2640−2651.
(62) Tretinnikov, O. N.; Ohta, K. Conformation-Sensitive Infrared Bands and Conformational Characteristics of Stereoregular Poly(Methyl Methacrylate)s by Variable-Temperature FTIR Spectroscopy. *Macromolecules* **2002**, *35*, 7343−7353.
(63) Krobok, M. P.; Johannsen, P. G.; Holzapfel, W. B. Raman and FTIR Study of NaOH and NaOD Under Pressure. *J Phys.: Condens. Matter* **1999**, *4*, 8141−8150.
(64) Agoston, P.; Albe, K. Thermodynamic Stability, Stoichiometry, and Electronic Structure of Bcc-$In_2O_3$ Surfaces. *Phys. Rev. B* **2011**, *84*, No. 045311.
(65) Cheng, X.-L.; Jiang, J.-S.; Jiang, D.-M.; Zhao, Z.-J. Synthesis of Rhombic Dodecahedral $Fe_3O_4$ Nanocrystals with Exposed High-Energy {110} Facets and Their Peroxidase-like Activity and Lithium Storage Properties. *J. Phys. Chem. C* **2014**, *118*, 12588−12598.
(66) Niu, W.; Zhang, L.; Xu, G. Shape-Controlled Synthesis of Single-Crystalline Palladium Nanocrystals. *ACS Nano* **2010**, *4*, 1987−1996.
(67) Niu, W.; Zheng, S.; Wang, D.; Liu, X.; Li, H.; Han, S.; Chen, J.; Tang, Z.; Xu, G. Selective Synthesis of Single-Crystalline Rhombic Dodecahedral, Octahedral, and Cubic Gold Nanocrystals. *J. Am. Chem. Soc.* **2009**, *131*, 697−703.
(68) Shavel, A.; Liz-Marzán, L. M. Shape Control of Iron Oxide Nanoparticles. *Phys. Chem. Chem. Phys.* **2009**, *11*, 3762−3766.
(69) Marcus, Y.; Hefter, G. Ion Pairing. *Chem. Rev.* **2006**, *106*, 4585−4621.
(70) Marks, L. D.; Peng, L. Nanoparticle Shape, Thermodynamics and Kinetics. *J. Phys.: Condens. Matter* **2016**, *28*, No. 053001.
(71) Herring, C. Some Theorem on the Free Energies of Crystal Surface. *Phys. Rev.* **1951**, *82*, 87−93.


https://dx.doi.org/10.1021/acs.chemmater.0c03281
*Chem. Mater.* 2020, 32, 9347−9354